Supporting Information

Microfluidic Screening of Electrophoretic Mobility Shifts Elucidates Riboswitch Binding Function

Kelly Karns[a,] Jacob M. Vogan[b], Qian Qin[c], Scott F. Hickey[c], Stephen C. Wilson[c], Ming C. Hammond[b,c] * and Amy E. Herr[a,d] *

[a]University of California, Berkeley–University of California, San Francisco Graduate Program in Bioengineering, [b]Department of Molecular & Cell Biology, [c]Department of Chemistry, and [d]Department of Bioengineering, University of California, Berkeley, CA 94720

SI Table of Contents

Figure S1: Quantitative Benefit of µMSA

The on-chip assay detected a 9.4% increase in SAM-I Bs riboswitch mobility with the addition of saturating concentrations of SAM ligand in a total analysis time of 3.2 min. A comparable 10.8% mobility shift took 17 hrs to run on a slab gel plus an additional hour to dry the gel before imaging (Figure S1). Percent mobility increase was calculated as $(\mu_{shifted} - \mu_{unshifted})/\mu_{unshifted}$. Total time to results for the microfluidic format includes 12.3 sec for each run to complete, a 20 sec load time for each run, a control and ligand sample, and triplicate runs for both samples in order to assess the statistical significance of the shift.

The repeatability and precision of microfluidic tools enables quantitative measurement of small differences in RNA peak mobility. Since diffusion scales with the square root of assay time, the rapid separation timescales of microfluidic formats (here 12.3 sec compared to 17 hours on a slab gel) lead to reduced diffusion and peak dispersion and enhanced signal to noise ratios. Since $\sigma^2 = \sigma_0^2 + 4Dt$ and separation resolution (R_s) is defined as $R_s = \Delta a/(2\sigma_1 + 2\sigma_2)$, where σ is peak width, σ_0 is starting peak width, D is the diffusion coefficient, t is time, Δa is the distance between the peaks, and σ_1 and σ_2 are the bound and unbound peak widths, respectively, we can derive the relationship between separation resolution, peak width, and time:

$$R_s = \frac{\Delta a}{2(\sqrt{\sigma_0^2 + 4D_1 t} + \sqrt{\sigma_0^2 + 4D_2 t})}$$

Assuming that σ_0 and D are the same on the slab gel and µMSA for both analytes (here assumed to be 100 µm and 1E-6 cm^2/sec, respectively), and given the measured assay times of 12.3 sec on-chip and 17 hours on a slab gel, we can see that for $R_s = 1$, Δa is 0.048859 cm on-chip and 1.979495 cm on a slab gel. 40-fold smaller differences in peak location (Δa) can be detected on-chip compared to a slab gel for the same peak R_s. This increased mobility resolution arises due to a reduction in diffusive peak dispersion with faster assay times.

Quantitative measurement of RNA peak mobility and assay repeatability also allows assessment of the statistical significance of a conformational change-induced mobility shift.

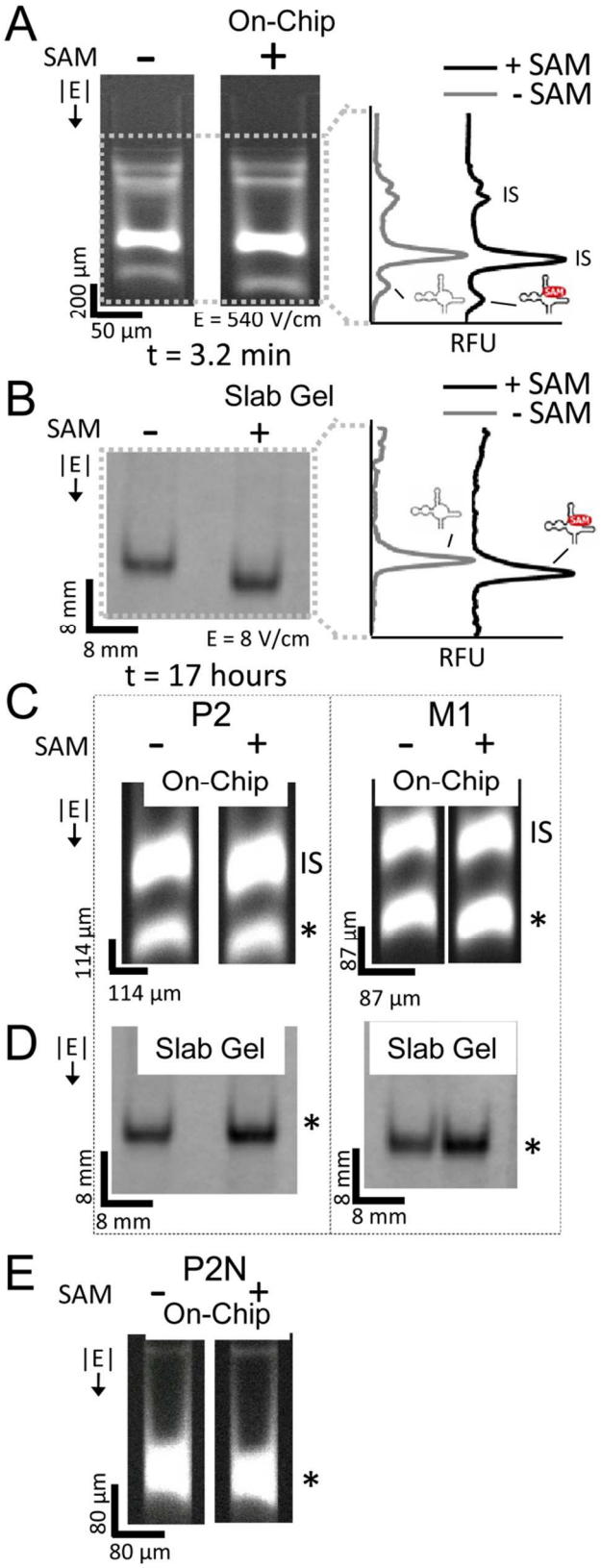

Figure S1: µMSA detects Bs SAM-I riboswitch shift in the presence of SAM ligand in 3.2 minutes **(A)** compared to 17 hours on a conventional slab gel **(B)**. No shift is observed for M1 or P2 mutants on-chip **(C)** or on a slab gel format **(D)**.

No shift is observed for P2N mutant on-chip **(E)** Riboswitch schematic indicates Bs SAM-I riboswitch peak. RNA mutants are indicated with '*' and IS indicates BSA internal standard. TBM10 used in gel and run buffers. RNA is labeled with AF_{488} (A and C) and FITC (B, D, and E).

Figure S2: Binding and Electrokinetic Transport Model

To derive a theoretical method by which to measure K_d for both slowly and rapidly interconverting riboswitch pairs in a microfluidic format, we modeled the mass transport of our system for varying association and dissociation rate constants. In PAGE mobility shift assays, the relevant transport includes binding reactions, diffusion, and electrophoretic migration. If we assume first order Langmuir binding, the concentration distributions of free riboswitch (c_A), bound riboswitch (c_B), and free ligand (c_L) during electrophoretic separation are expressed as a system of dimensionless partial differential equations:

$$\frac{\partial c_A}{\partial \bar{t}} = \frac{\overline{D_A}}{Pe}\frac{\partial^2 c_A}{\partial \bar{x}^2} - \overline{\mu_A}\frac{\partial c_A}{\partial \bar{x}} - Da_{on}c_A + Da_{off}c_B \quad (1)$$

$$\frac{\partial c_B}{\partial \bar{t}} = \frac{\overline{D_B}}{Pe}\frac{\partial^2 c_B}{\partial \bar{x}^2} - \overline{\mu_B}\frac{\partial c_B}{\partial \bar{x}} + Da_{on}c_A - Da_{off}c_B \quad (2)$$

$$\frac{\partial c_L}{\partial \bar{t}} = \frac{\overline{D_L}}{Pe}\frac{\partial^2 c_L}{\partial \bar{x}^2} - \overline{\mu_L}\frac{\partial c_L}{\partial \bar{x}} - Da_{on}c_A + Da_{off}c_B \quad (3)$$

where $\bar{t} = t\mu_A E/L$, $\bar{x} = x/L$, $\overline{D} = D_i/D_o$, $\bar{\mu} = \mu_i/\mu_A$, L is the separation length, E is the applied electric field, μ is analyte mobility, t is time, and D_o is the characteristic diffusivity. In this form, we see that the Peclet number, Pe, gives the ratio of electromigration to diffusion timescales and is defined as $E\mu_A L/D_o$. The two Damkohler numbers, Da_{on} and Da_{off} give the ratio of the migration to the reaction timescales and are defined as $Da_{on} = k_{on}Lc_L/E\mu_A$ and $Da_{off} = k_{off}L/E\mu_A$ where k_{on} and k_{off} are the association and dissociation rate constants, respectively. A large Damkohler number indicates the reaction is happening faster than electromigration along the channel (Da_{on} and $Da_{off} > 1$).

Using a numerical initial-boundary value partial differential equation solver in Matlab, we solved these equations simultaneously for a given set of parameter values. Initial analyte concentrations were assumed to be overlapping equilibrium Gaussian peaks at the beginning of the separation channel with 200 μm peak widths. Total RNA concentration ($c_A + c_B$) was 1 μM and ligand concentration (c_L) was 1 μM. Peak mobilities of 1.06338E-5 cm^2/Vs, 1.18E-5 cm^2/Vs, and 1.2E-5 cm^2/Vs, a separation length of 4 mm, and an applied electric field of 500 V/cm was assumed to match experimental conditions. For separations where either peak had a measured concentration < 0.01 μM at L, only one peak was assumed and R_s was undefined. In these regimes, all RNA was either bound or unbound.

In rationally designing the assay, we utilize the separation resolution metric (R_s) which reports the ability to resolve shifted riboswitch populations (i.e., ligand-bound) using PAGE. The two Da metrics allow us to compare the migration to the reaction timescales.

Figure S2 details anticipated R_s values (for the bound and unbound riboswitch peaks) across a biologically relevant range of electrophoretic and reactive transport conditions and shows that R_s is

dependent on both Da_{on} and Da_{off}. In Figure S2, undefined R_s regimes were represented as R_s of 0. Since $\frac{Da_{off}}{Da_{on}} = \frac{K_D}{c_L} = \frac{c_A}{c_B} = \frac{k_{off}}{k_{on}c_L}$, peak overlap, measured by R_s, is determined by the magnitudes of Da_{on} and Da_{off}, while peak height depends on the ratio of Da_{off}/Da_{on}. Because of the higher electric field strengths attainable in a microfluidic channel (~800 V/cm on-chip vs. ~20 V/cm on a slab gel), µMSA allows access to 40× lower Da_{on} and Da_{off} values compared to slab gels for a given riboswitch-ligand pair. Thus, improved separation resolution is expected between unbound and bound riboswitch peaks on a microfluidic format compared to a slab gel. To compare the accessible Da_{on} and Da_{off} values for the two platforms, compare the microfluidic performance space (solid box in Figure S2) to that of the conventional slab gel (dashed box), here for a riboswitch-ligand pair with k_{on} = 1.5E-3 /µMsec and k_{off} =1.5E-5 /sec. The microfluidic format allows assay operation at Da_{on} < 1 and Da_{off} < 1, and therefore allows two peaks to be resolved at intermediate ligand concentrations for a given riboswitch-ligand pair (dark circle in Figure S2 where k_{on} = 1.5E-4/µMsec and k_{off} = 1.5E-4/sec) where they could not be in a slab gel format (dark diamond in Figure S2 for the same k_{on} and k_{off} values).

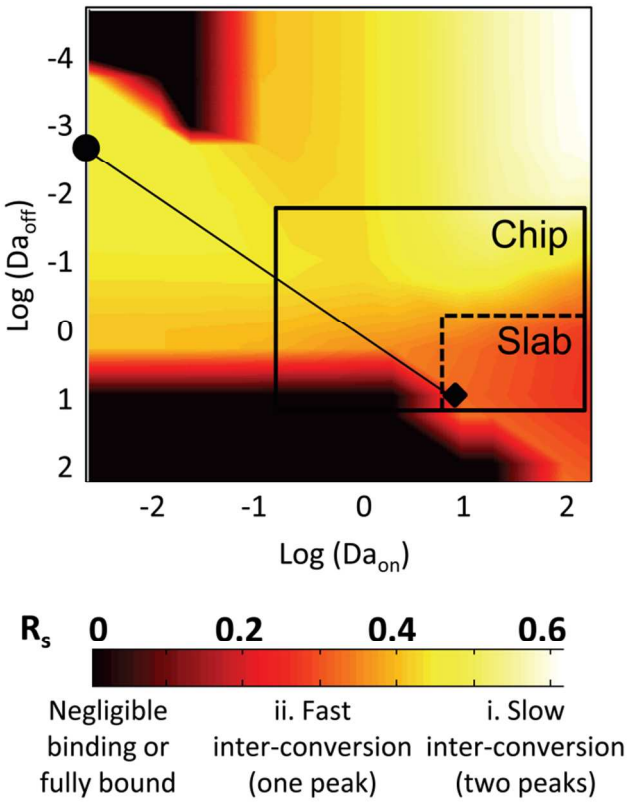

Figure S2: Separation resolution of bound and unbound riboswitch populations is dependent on Da. Tuning assay conditions such as applied voltage and ligand concentration allows the microfluidic format to access a wider range of Daon and Daoff values. Compare the microfluidic performance space (solid box) to that of the conventional slab gel (dashed box), here for a riboswitch-ligand pair with kon = 1.5E-3 /µMsec (similar to kon of 2AP and 70 pbuE riboswitch[1]) and koff =1.5E-5 /sec (similar to FMN + 165 ribD riboswitch[2]). The microfluidic format allows assay operation at Daon < 1 and Daoff < 1, and therefore allows two peaks to be resolved for a given riboswitch-ligand pair (dark circle where kon = 1.5E-4/µMsec and koff = 1.5E-4/sec) where they could not be in a slab gel format (dark diamond for the same kon and koff values).

Figure S2 illustrates the various regimes that exist for differing association, dissociation, and electromigration timescales. The two Da metrics allow us to compare the migration to the reaction timescales. A large Damkohler number indicates the reaction is happening faster than electromigration along the channel (Da_{on} and $Da_{off} > 1$). In the case when $Da_{on} > 1$ and $Da_{off} < 1$ or $Log(Da_{on}) > 0$ and $Log(Da_{off}) < 0$, k_{on} is high and the timescale for binding is very fast, while k_{off} is low and the timescale for dissociation is very slow relative to the electromigration timescale. In Figure S2, this regime is in the upper right hand corner and we see that the peaks are well resolved with a maximum R_s. In this case, there is minimal interconversion between bound and unbound forms of the riboswitch owing to the rapid binding and slow dissociation times – bound RNA remains bound during the separation. In this regime, two peaks are resolved from each other which represent the bound and unbound populations and the K_d can be extracted by tracking the amount of bound RNA as ligand concentration is increased.

In the case when $Da_{on} > 1$ and $Da_{off} > 1$ or $Log(Da_{on}) > 0$ and $Log(Da_{off}) > 0$, k_{on} is high and the timescale for binding is very fast. Meanwhile k_{off} is also high and the timescale for dissociation is also very fast relative to the electromigration timescale. In Figure S2, this regime is in the lower right hand corner and we see that the peaks are poorly resolved with a minimum R_s (while still retaining both bound and unbound forms in the system). In this case, there is rapid interconversion between bound and unbound forms of the riboswitch during the separation owing to the rapid binding and dissociation times relative to the electromigration times. Here, ligand that is dissociated during the separation is quickly rebound by free RNA in the plug. In this regime, the two peaks are predicted to overlap, yielding a single riboswitch peak which represents the fraction bound and the K_d can be extracted by tracking the mobility of the single peak as ligand concentration is increased. In both regimes, free ligand will move with a fast electrophoretic mobility, owing to its small size, but the observed interconversion regimes will occur independent of ligand mobility.

Third and fourth regimes also exist where 1) binding is so slow that only unbound RNA exists and 2) dissociation is so slow that only bound forms of the riboswitch exist; however, these regimes are not observed here.

Figure S3: Critical Separation Resolution Calculation

The absolute R_s value extracted from the computational model is dependent on the difference in absolute mobility values given for the bound and unbound riboswitch peaks, electric field and separation time.[3] The proof for this is given by the following equations which describe peaks as illustrated in Figure S3:

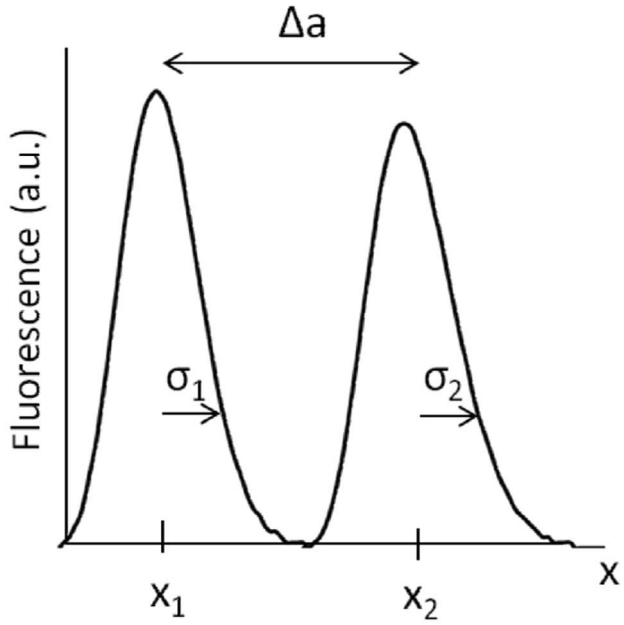

Figure S3: Schematic of the fluorescence signal of two resolved RNA bands. σ positions in the figure are approximate

$$R_s = \frac{\Delta a}{4\sigma}$$

Since $u = \mu E$ and u = x/t where u is peak velocity, μ is peak mobility, x is peak position, t is time, and E is the applied electric field,

$$\mu = \frac{x}{tE} \quad \text{and} \quad \Delta\mu = \frac{\Delta x}{tE}$$

Since Δx = Δa as shown in the figure above,

$$R_s = \frac{\Delta\mu tE}{4\sigma}$$

Therefore, the absolute separation resolution extracted from the model is dependent on the values of these variables as entered into the model. To match the model to separation conditions measured on-chip, peak mobilities of 1.06338E-5 cm^2/Vs, 1.18E-5 cm^2/Vs, and 1.2E-5 cm^2/Vs, a separation length of 4 mm, and an applied electric field of 500 V/cm was assumed. A characteristic diffusion coefficient (which will impact σ) was assumed to be 1E-6 cm^2/s (measured value for GFP protein in a 4%T polyacrylamide gel) and then weighted by the relative mobility of the bound and unbound peaks to give 0.169272E-6 cm^2/sec and 1E-6 cm^2/s for unbound and bound peaks, respectively. With these values, the model gives a maximum R_s of 0.6 at 4 mm separation distance, which matches experimental values.

Figure S2 shows that, for the assay and analyte conditions measured here, R_s of 0.5 acts as a critical threshold. Above R_s of 0.5, two peaks are observed and slow interconversion is apparent. Below R_s of 0.5, a single peak is observable and rapid interconversion is apparent.

Figures S4 and S5: In-line Probing Assays

Ligand binding analysis was performed following standard in-line probing procedures[4] with modifications to the buffer conditions to match the conditions used for native PAGE. Briefly, 5'-^{32}P radiolabeled RNAs were incubated in TBM10 or TBM1 buffer with 0-5 µM of SAM ligand for the *B. subtilis* SAM-I riboswitch or 0-500 nM of SAM ligand for the *P. irgensii* SAM-I riboswitch. After 43 h at room temperature, the reaction samples were loaded onto a 10% urea-PAGE gel made with TBE buffer (90 mM Tris, 90 mM Boric acid, 1 mM EDTA, pH 8.3) and the gel was run at constant 40 W for 2-3 h at room temperature. After drying at 80 °C for 2 h, the gel was scanned using the Typhoon laser-scanning system (GE Healthcare) on the phosphorimager setting.

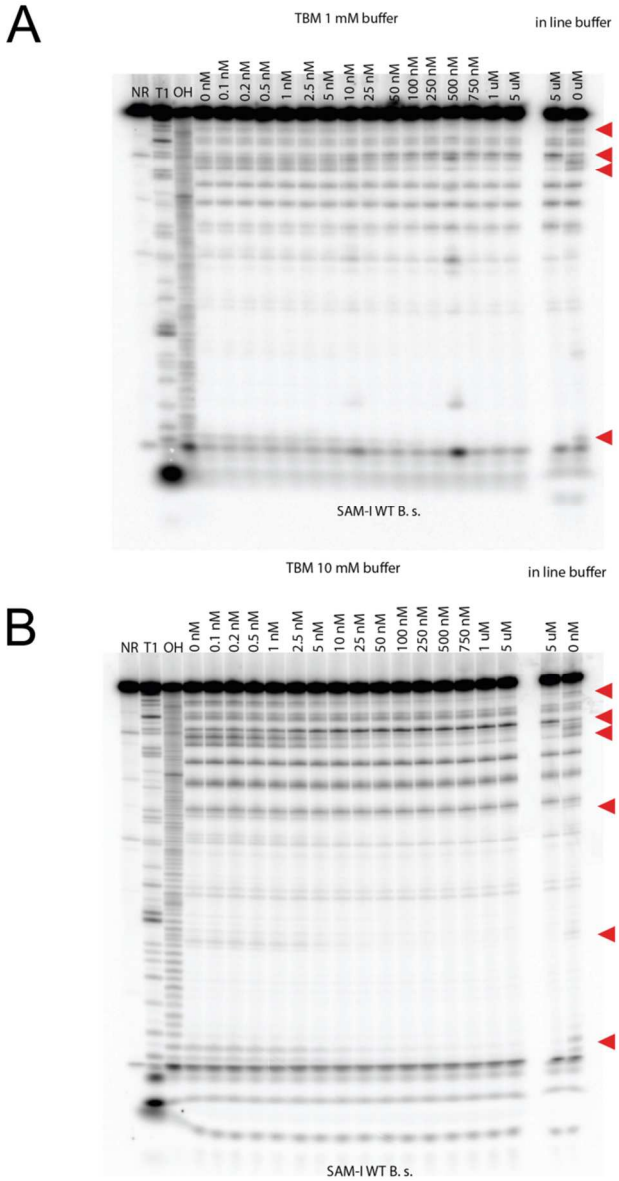

Figure S4: Phosphorimager scans of in-line probing gels for Bs SAM-I riboswitch in 1x TB buffer with (A) 1 mM Mg2+ and (B) 10 mM Mg^{2+} show the pattern of spontaneous cleavage. Sites of modulation that were analyzed are marked as red triangles. NR = no reaction, T1 = partial digest with RNase T1, -OH = partial digest with alkali. Control samples using standard in-line buffer (50 mM Tris-HCl, 20 mM $MgCl_2$, 100 mM KCl, pH 8.3) show the same modulation pattern.

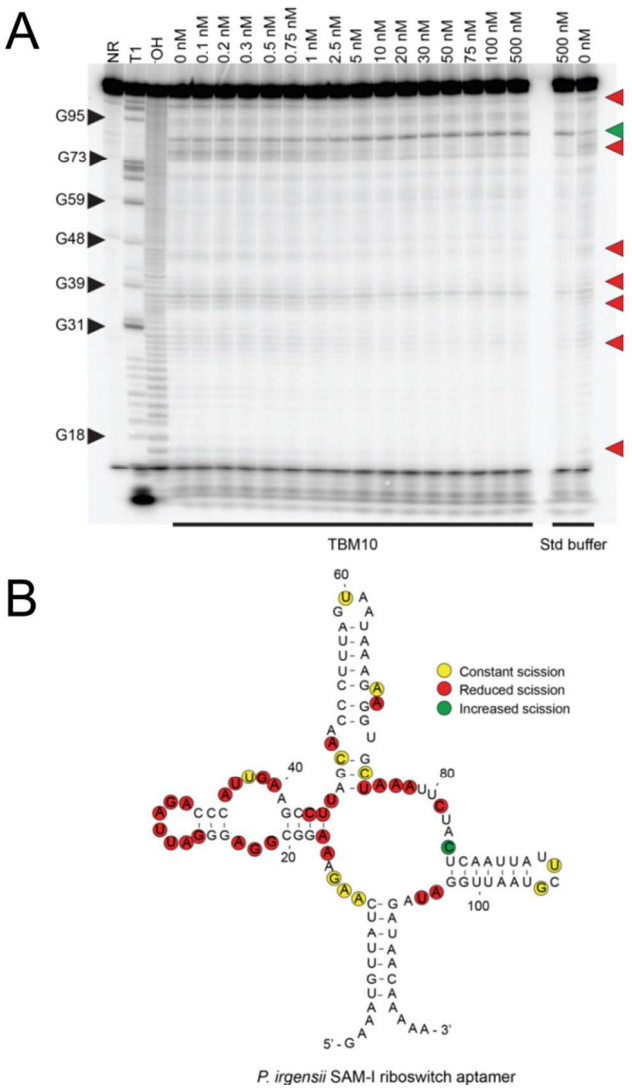

Figure S5: Phosphorimager scans of in-line probing gels for Pi SAM-I riboswitch in 1x TB buffer with (A) 10 mM Mg^{2+} show the pattern of spontaneous cleavage. Sites of modulation that were analyzed are marked as red triangles (reduced scission) or green triangles (increased scission). NR = no reaction, T1 = partial digest with RNase T1, -OH = partial digest with alkali. Control samples using standard in-line buffer (50 mM Tris-HCl, 20 mM $MgCl_2$, 100 mM KCl, pH 8.3) show the same modulation pattern. (B) Sequence and secondary structure model for P. irgensii SAM-I mapped with the in-line probing pattern.

Figure S6: Slab Gel Mobility Resolution is Dependent on Well Size

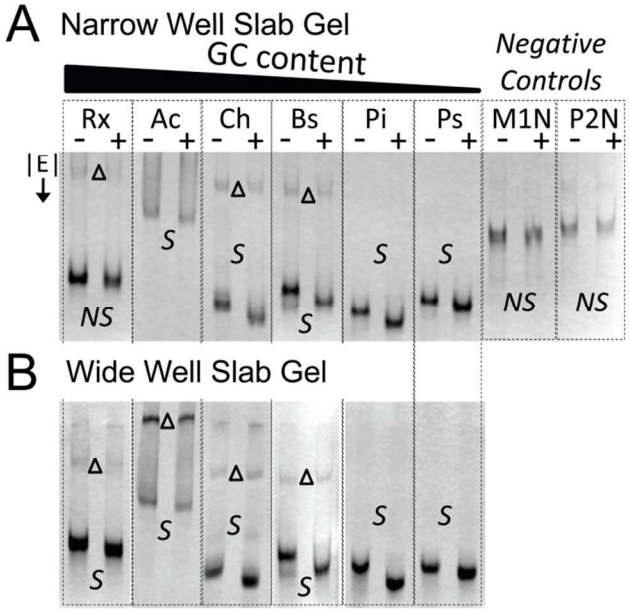

Figure S6: Mobility shift resolution on a slab gel is dependent on well size. No mobility shift is detected for Rx when narrow sample wells are used (A), while a mobility shift is detected for Rx when well size is increased (B). Narrower sample loading wells allow for increased parallelization of sample runs, but sacrifice resolution of mobility shifts by increasing injection band dispersion. 'S' indicates a shift and 'NS' indicates no shift. M1N and P2N mutants do not demonstrate a shift, as expected. Upper bands in slab gel ('Δ') appear to be non-binding RNA conformers. Slab gel E = 8 V/cm, on-chip E = 240 V/cm. 1× TB + 10 mM Mg^{2+} in gel and run buffers.

Reagents and Oligonucleotides

10× TB buffer was made by adding 900 mM tris base (Thermo Fisher Scientific, Waltham, MA), 890 mM boric acid (VWR, Radnor, PA), and $MgCl_2$ (EMD Millipore, Darmstadt, Germany), and/or KCl (Sigma-Aldrich, St. Louis, MO), as appropriate to 30 mL water and titrating to pH 8.5 with 1 M NaOH (Thermo Fisher Scientific).

Bovine-serum albumin (BSA, Sigma Alderich), phosphorylase B (PB, Sigma-Aldrich), α-lactalbumin (α-lact, Sigma-Aldrich), and trypsin inhibitor (TI, Life Technologies, Grand Island, NY) were used as internal standards. Internal standards were labeled in-house with AlexaFluor 488 or 633 dyes (LIF system only) according to the manufacturer's instructions (Life Technologies). Protein concentration and degree of labeling were measured using a NanoDrop (Thermo Fisher Scientific).

DNA oligonucleotides were purchased from ElimBio (Hayward, CA) or Integrated DNA Technologies (San Diego, CA). Sodium periodate, fluorescein-5-thiosemicarbazide and *S*-adenosylmethionine (SAM) were purchased from Sigma Aldrich. AlexaFluor 488 hydrazide sodium salt, and AlexaFluor 633 hydrazide bis(triethylammonium) salt were purchased from Invitrogen.

Preparation of DNA Constructs

DNA templates for RNA constructs corresponding to computationally predicted wild-type riboswitch sequences from different organisms (*Bacillus subtilis*, *Polaribacter irgensii*, *Acidothermus cellulolíticus*, *Carboxydothermus hydrogenoformans*, *Polaribacter spp.*, and *Rubrobacter xylanophilus*) were either amplified by PCR from the genomic DNA or purchased from IDT as a single-stranded oligonucleotide and amplified by PCR. The resulting PCR products were cloned into TOPO vector (Invitrogen) and sequence confirmed. DNA templates for P2 and M1 mutants were generated by PCR extension of overlapping primers containing the desired mutations, followed by cloning into TOPO vector and sequence confirmation. M1N and P2N are M1 and P2 mutants with additional natural flanking sequences (+27 nt upstream at the 5' end and +25 nt downstream at the 3' end). They were constructed by Quikchange mutagenesis using WTN as the template (124 yitJ+natural flanks). Sequences for all DNA templates used in the study are provided below and sequences for the primers are provided in Table S1.

Preparation of 3' End Labeled Fluorescent RNAs

RNAs were transcribed *in vitro* using standard protocols[5] from DNA templates containing the extended T7 promoter sequence generated by PCR. Briefly, transcription reactions were performed using 2 µg DNA template and T7 RNA polymerase (expressed from pT7-911 plasmid in BL21 Star and purified using Ni-NTA by QB3 MacroLab Facility, UC Berkeley) at 37 °C for 2-3 h. RNAs were purified by separation on a 6% denaturing PAGE gel, extracted from gel slices using crush-soak buffer (10 mM Tris, pH 7.5, 200 mM NaCl, 1 mM EDTA, pH 8.0), and precipitated in ethanol at -20 °C. After decanting the ethanol, RNAs were air-dried and redissolved in water. RNA concentrations were measured by the absorbance at 260 nm using a micro-volume UV-Vis spectrophotometer (Nanodrop ND-8000).

Fluorophore dyes (fluorescein, AlexaFluor 488, or AlexaFluor 633) were conjugated to the RNAs following standard procedures for 3' end labeling[6]. Briefly, the dialdehyde of the 3' end ribose sugar was generated by oxidation of the RNAs (0.1-1 nmol) using freshly prepared 2.5 mM sodium periodate in 100 mM sodium acetate buffer, pH 5.0 at 0 °C for 50 min. The oxidation reaction was quenched by addition of excess ethanol to precipitate the RNA dialdehydes at -20 °C. After removal of the ethanol and air-drying, RNAs were immediately dissolved in 100 mM sodium acetate buffer, pH 5.0 and incubated with excess reactive fluorophore reagent (fluorescein-5-thiosemicarbazide, AlexaFluor 488 hydrazide, or AlexaFluor 633 hydrazide) at 1 mM concentration at 0 °C overnight in the dark. The RNAs were recovered by ethanol precipitation followed by gel purification as described above.

The labeling efficiency for each fluorophore dye was determined as follows. The absorbance at the fluorophore excitation wavelength (494 nm for fluorescein, 633 nm for AlexaFluor 633) was measured and this value was divided by the appropriate extinction coefficient (68,000 M^{-1} cm^{-1} for fluorescein[7], 160,000 M^{-1} cm^{-1} for AlexaFluor 633[8], and 71,000 M^{-1} cm^{-1} for AlexaFluor 488[9]) to yield the fluorophore dye concentration. The RNA concentration was determined by measurement of the UV absorbance at 260 nm after thermal hydrolysis to yield the nucleotide monophosphates and employing Beer's law and

the extinction coefficient of the nucleotide monophosphates to calculate the concentration of the known RNA sequence. The labeling efficiency was calculated as moles of fluorophore dye per moles of RNA by taking the ratio of the concentrations. The average RNA labeling efficiency was 75% using fluorescein-5-thiosemicarbazide (5 independent samples) and 30% using AlexaFluor 633 hydrazide bis(triethylammonium) salt (7 independent samples).

Microfluidic Device Fabrication

Gel precursor solutions were prepared by diluting 30% (w/v) acrylamide/bis-acrylamide (Sigma Aldrich, St. Louis, MO) with the appropriate 10× TB buffer and water to achieve the desired total acrylamide concentration (3%T, 10%T or 12%T) in 1× TB buffer with 0.2% (w/v) water-soluble photoinitiator 2,2-azobis[2-methyl-N-(2-hydroxyethyl) propionamide] (VA-086, Wako Chemicals, Richmond, VA). Precursor solutions were degassed using sonication (~5 min) before use. The small pore size precursor solution was introduced into the channels using capillary action and the chip was aligned over a transparency mask with a 4 mm x 500 µm opening (designed in-house and fabricated by Fineline Imaging, Colorado Springs, CO) so that the region of the separation channel directly downstream of the injection junction was exposed. The masked device was seated on an inverted Nikon Diaphot 200 microscope (Melville, NY), drops of viscous 5% (w/v) 2-hydroxyethyl cellulose (HEC) (Sigma Aldrich, St. Louis, MO) were applied to each well to suppress bulk fluid flow, and the device was allowed to equilibrate for 5 min. UV light from a Hamamatsu LightningCure LC5 UV light source (Hamamatsu City, Japan) was directed into the light path of the microscope and through a UV transmission objective lens (UPLANS-APO 4x, Olympus, Center Valley, PA). The masked chip was exposed to UV light for 270 sec at a beam intensity of ~1.65 mW/cm^2 (measured with a UV513AB Digital Light Meter, General Tools, New York, NY). Unpolymerized precursor solution was replaced with 3%T precursor solution by sequentially applying vacuum to wells S, SW, and B (Figure 1). The entire chip was then flood exposed for 8 min at ~8.5 mW/cm^2 on a 100 W filtered mercury UV lamp (UVP B100-AP, Upland, CA) a distance of 5 in from the chip.

Epi-Fluorescent Microscope Set-up and Image Processing

Migration and concentration distributions of separating fluorescent analytes were measured via an IX-70 inverted epi-fluorescent microscope equipped with a 100 W mercury arc lamp (Olympus, Center Valley, PA), 10× objective (UPlanFL, NA 0.3, Olympus, Center Valley, PA), 0.63× demagnifier (Diagnostic Instruments Inc., Sterling Heights, MI), and a filter cube optimized for GFP (XF100-3, Omega Optical, Brattleboro, VT). Sequential full-field image capture was performed using a 1392×1030 Peltier-cooled charge-coupled device (CCD) camera (CoolSNAP HQ2, Roper Scientific, Trenton, NJ), 75 msec exposure time, and 4×4 pixel binning.

Full-field image post-processing was done with ImageJ (National Institutes of Health). Intensity profiles of the separation channel were generated using a standardized ROI along the length of the separation channel. FITC-labeled SAM-I Bs RNA was used at 12 nM and 158 nM Alexa fluor 488-labeled BSA was

used as an internal standard (Figure 2A, Figure S1). Buffer screening studies utilized 93 nM of FITC-labeled SAM-I Bs RNA and 400 nM Alexa Fluor 488-labeled TI and 424 nM Alexa Fluor 488-labeled PB as internal standards (Figure 4). In the SAM-I Pi mobility shift assay, 374 nM FITC-labeled SAM-I Pi riboswitch was used with 400 nM Alexa Fluor 488-labeled TI and 424 nM Alexa Fluor 488-labeled PB as internal standards (Figure 5A). On-chip gel shifts were assessed by extracting electropherograms 2 mm downstream of the injection junction, aligning the internal standard peaks for all runs for a given sample, and fitting a nonlinear Gaussian peak fitting algorithm (GaussAmp) using OriginPro 8.5 (OriginLab, Northampton, MA) in order to measure the peak center. RNA peak mobility was calculated as peak velocity ÷ applied electric field. Statistical significance was determined for triplicate runs using a two-tailed t-test with $p < 0.05$. Percent mobility increase was calculated as $(\mu_{shifted} - \mu_{unshifted})/\mu_{unshifted}$.

Laser Induced Fluorescence (LIF) System Operation

The LIF system was built using a 25 LHP 991-249 HeNe laser (Melles Griot, Carlsbad, CA) and IX70 inverted epi-fluorescence microscope (Olympus, Center Valley, PA). Laser light was passed through a 15× beam expander (BE 15M, Thorlabs, Newton, NJ) before passing into the back of the epi-fluorescence microscope and through XF2022 dichroic and XF3030 emission filters (Omega Optical, Brattleboro, VT). The filter sets were chosen to not contain an excitation filter; thus allowing 100% of excitation signal to pass to the sample and 75% of Alexa Fluor 633 dye emission signal to be collected. PA gel-containing glass chips were seated on the LIF microscope stage and pipette tips were fitted into the reservoir access holes to augment sample wells. Sample and buffer were pipetted on-chip and the assay was run as before. A clip-on goose neck lamp was used as brightfield illumination for chip alignment. All microfluidic K_d measurements were collected at 1 mm separation distance on 3-12%T separation gels. SAM-I Bs riboswitch K_d was measured in TBM1 buffer (90 mM Tris, 89 mM Boric acid, 1 mM $MgCl_2$, pH 8.5) using 1 nM Alexa Fluor 633-labeled SAM-I Bs RNA, 6.3 nM PB, and varying SAM ligand concentrations. SAM-I Bs riboswitch K_d was measured in TBM10 buffer (90 mM Tris, 89 mM Boric acid, 10 mM $MgCl_2$, pH 8.5) using 870 pM Alexa Fluor 633-labeled SAM-I Bs RNA, BSA, 22.4 nM α-lact, and varying SAM ligand concentrations. SAM-I Pi riboswitch K_d was measured in TBM10 buffer (90 mM Tris, 89 mM Boric acid, 10 mM $MgCl_2$, pH 8.5) using 970 pM Alexa Fluor 633-labeled SAM-I Pi RNA (51% degree of labeling), phosphorylase B as an internal standard, and varying SAM ligand concentrations. The fluorescence signal from separating peaks was collected by a D-104 photomultiplier tube (Photon Technology International, Birmingham, NJ) and integrated with the computer with a SCB-68 shielded I/O connector block and DAQ device (National Instruments, Austin, TX). LabView (National Instruments) was used to collect voltage data. Laser safety glasses effective at 633 nm were worn at all times while operating the LIF system.

Selection of Analyte Concentrations for μMSA K_d Measurements

For a bimolecular binding reaction, we can rearrange the dissociation constant equation to get an equation for the fraction of analytes that are bound:

$$\frac{[AB]}{[A]_{TOTAL}} = \frac{[B]}{[B] + K_D}$$

Here, $[AB]/[A]_{TOTAL}$ represents the fraction of A that is bound and [B] is the concentration of free ligand in solution. Therefore, measuring K_d can be done by keeping the concentration of A in the reaction constant and varying the amount of B added. At each concentration of B, the concentrations of the AB complex and free B are measured.[10] In theory, any concentration of A can be used in this experiment. However, in practice and in the experiments performed in this study, it is impossible to measure free B without labeling or modifying the SAM ligand. The total concentration of B in a reaction is easily known since it is the amount of ligand added to the system. When $[A]_{TOTAL} << K_d$, the total concentration of B is equal to the sum of the concentrations of free and bound B. Under these conditions, the amount of B bound in the AB complex will be only a small fraction of the total B and free [B] is approximately equal to $[B]_{TOTAL}$. Therefore, if $[A]_{TOTAL} << K_d$, the total concentration of B added to each reaction can be plotted versus fraction bound and the K_d can be determined using the equation above.[10]

In this work, we sought to introduce a riboswitch functional screening assay optimized for measurement of K_d. Since the RNA concentration must be significantly less than the expected K_d value to measure K_d, analytical sensitivity was an important design specification for this screening assay.

Mobility and Peak Height Calculations for Microfluidic K_d Measurements

The mobility used to measure K_d with μMSA is a relative mobility which reflects the observed mobility shift relative to the maximum shift observed in saturating ligand conditions. As a result of the rapid interconversion rate of the riboswitch-ligand pair, this relative mobility metric corresponds to the population-average of bound riboswitches and can be used to extract the percentage bound and the K_d value. As such, the absolute mobility of the RNA does not impact the derived binding constant.

Relative RNA mobility was calculated as the difference in RNA and internal standard mobility at each ligand concentration tested. Electropherograms were created 1 mm downstream of the injection junction and a Gaussian peak was fitted using OriginPro 8.5 in order to measure the time for the center of the peak to reach 1 mm. For rapidly interconverting riboswitch ligand pairs in TBM1 buffer, relative mobility = $\Delta\mu = (x/E)/(t_{RNA} - t_{IS})$ where IS is phosphorylase B internal standard, x is 1 mm separation distance, E is the measured applied E-field, and t is the measured time for the center of each band to travel 1 mm. In TBM10 buffer, relative mobility = maximum $\Delta\mu$ - $(x/E)/(t_{RNA} - t_{IS})$ where IS is BSA internal standard. Because BSA travels faster than SAM-I Bs RNA, $\Delta\mu$ was subtracted from the maximum $\Delta\mu$ in order to see an increasing trend similar to that of TBM1 buffer. Fitted variables for the SAM-I Bs riboswitch were β_1 = 5.9161E-6, β_3 = 34934E-6, K_d = 25.3 nM in TBM1 buffer and β_1 = 4.3337E-6, β_3 = 1.9674E-6, K_d = 3.14123 nM in TBM10 buffer. Fitted variables for the SAM-I Pi riboswitch were β_1 = 0.18408 ± 0.02589, $\beta_3 = 0.0735 \pm 0.01447$, $K_d = 1.0 \pm 0.2$ nM in TBM10 buffer.

Peak height was used to quantify the detectable signal from the bound Pi riboswitch peak. Peak height is routinely used as a proxy for bound peak area in the creation of dose response curves for antibody-

antigen binding pairs.[11,12] Since separated RNA peaks are represented by a Gaussian curve owing to diffusive dispersion, the equation for a Gaussian curve is:

$$f(x) = he^{\frac{-(x-b)^2}{2\sigma^2}}$$

where h is peak height, b is the position of the peak center, and σ is peak variance. The total concentration is therefore the area under the Gaussian curve, or the integral of f(x). This is equal to:

$$concentration = h\sigma\sqrt{2\pi}$$

Therefore, assuming that the peak width (σ) doesn't change appreciably, the concentration is proportional to peak height, h. This is a valid assumption because the peaks are analyzed at the same separation time in creating the dose response curve and therefore have experienced approximately equal diffusive dispersion (since diffusion scales with $\sqrt{time}$).

We used bound peak height in the computational model (Figure 1C) to demonstrate our ability to extract K_d for slowly interconverting riboswitches. Here, the plot is of bound peak height vs. increasing SAM ligand concentration and a K_d of 60 nM is extracted. To maintain consistency and also because of the reasons outlined in the proof above, we also used peak height for the experimental data to extract K_d for Pi SAM-I riboswitch.

μMSA Screening of Candidate Riboswitch Functionality

Fluorescein-labeled SAM-I mutant riboswitches M1 and P2 were run on-chip as negative controls at 304 nM and 360 nM, respectively. 400 nM Alexa Fluor 488-labeled TI and 424 nM Alexa Fluor 488-labeled PB were used as internal standards. FITC-labeled SAM-I Rx, Ac, and Ch riboswitches were at 150 nM. FITC-labeled SAM-I Pi and Ps riboswitches were at 412 nM and 260 nM, respectively. Slab gels were run with no internal controls and M1N and P2N mutant riboswitches as negative controls.

Slab Gel Native PAGE Assays

While protected from light, 1-3 pmol fluorescently labeled RNA in 20 μL of TBM10 buffer was renatured by heating to 70 °C on a heat block for 3 min followed by a quick table-top centrifugation and slow cooling to room temperature for 1 h. Renaturation of the RNA was performed either in the presence (500 nM or 5 μM) or absence of SAM. Glycerol was added the sample to 5-10% v/v prior to loading onto a 10% acrylamide/bisacrylamide (29:1) gel made with TBM10 buffer, which had been pre-equilibrated with TBM10 buffer for at least 1 h. The gel was run with recirculating TBM10 buffer at 4 °C at 200 V (electric field of 8 V/cm) for 17-20 h in the dark. After drying at 70 °C for 30 min using the Bio-Rad model 583 gel dryer connected to a Welch DryFast vacuum pump, the gel was scanned using the Typhoon laser-based scanning system (GE Healthcare) at the excitation and emission wavelength settings

appropriate to the fluorophore dye used (ex/em 532/526SP nm for fluorescein, either 532/526SP or 488/520BP AlexaFluor 488, and 633/670 nm for AlexaFluor 633). If used, internal standards were diluted to match the fluorescence intensity of the labeled RNA and added immediately prior to sample loading. For experiments performed at 1 mM Mg^{2+}, TBM1 buffer was used in the sample reaction, in the gel, and as the running buffer. For experiments performed at different RNA to ligand ratios, the concentration of RNA was kept constant (120 nM for fluorescein-labeled *B. subtilis* SAM-I riboswitch and 120 nM for fluorescein-labeled *P. irgensii* SAM-I riboswitch) and the concentration of the SAM ligand was added in the ratios shown in the figure.

Sequences of DNA Constructs

The extended T7 promoter sequence is shown in lower caps. Additional G nucleotides to enhance transcription initiation are bolded. Mutations are shown in red. Underlined are the natural flanking sequences.

Bacillus subtilis 124 yitJ SAM-I aptamer domain (Bs):

Wild type[13]

ccaagtaatacgactcactata**GG**GTTCTTATCAAGAGAAGCAGAGGGACTGGCCCGACGAAGCTTCAGCAACCGGTGTA
ATGGCGATCAGCCATGACCAAGGTGCTAAATCCAGCAAGCTCGAACAGCTTGGAAGATAAGAAGAG

P2 (mutation at P2 stem that disrupts pseudoknot formation)[14]

ccaagtaatacgactcactata**GG**GTTCTTATCAAGAGAAGCAGAGGGACTCCCCCGACGAAGCTTCAGCAACCGGTGTA
ATGGCGATCAGCCATGACCAAGGTGCTAAATCCAGCAAGCTCGAACAGCTTGGAAGATAAGAAGAG

M1 (mutation at P1/P2 junction that disrupts ligand binding but not folding)[13]

ccaagtaatacgactcactata**GG**GTTCTTATCAGAAGAAGCAGAGGGACTGGCCCGACGAAGCTTCAGCAACCGGTGTA
ATGGCGATCAGCCATGACCAAGGTGCTAAATCCAGCAAGCTCGAACAGCTTGGAAGATAAGAAGAG

P2N

ccaagtaatacgactcactata**GG**ACTTCCTGACACGAAAATTTCATATCCGTTCTTATCAAGAGAAGCAGAGG
GACTCCCCCGACGAAGCTTCAGCAACCGGTGTAATGGCGATCAGCCATGACCAAGGTGCTAAATCC
AGCAAGCTCGAACAGCTTGGAAGATAAGAAGAGACAAAATCACTGACAAAGTCTTCTT

M1N

ccaagtaatacgactcactata**GG**ACTTCCTGACACGAAAATTTCATATCCGTTCTTATCAGAAGAAGCAGAGG
GACTGGCCCGACGAAGCTTCAGCAACCGGTGTAATGGCGATCAGCCATGACCAAGGTGCTAAATCC
AGCAAGCTCGAACAGCTTGGAAGATAAGAAGAGACAAAATCACTGACAAAGTCTTCTT

Polaribacter irgensii 23-P SAM-I aptamer domain (Pi):

Genbank accession AAOG01000001.1, nucleotides 142961..142846

ccaagtaatacgactcactata**GG**GAAATGTTATCAAGAAAGGCGGAGGGATTAGACCCATTGAAGCCTTAGCAACCCTT
TAGTAATAAAGAAGGTGCTAAATTCTACTCAATTATTCGTAATTGGATAGATAACAAAAA

Rubrobacter xylanophilus DSM 9941 SAM-I aptamer domain (Rx):
Genbank genome accession CP000386.1, nucleotides 882034..882017
ccaagtaatacgactcactata**GG**GGGCGCTCATCGAGAGCGGTGGAGGGACGGGCCCTGCGAAGCCGCGGCAACCGG
CGGGCGGCGGACGCCCGCGCCAGGTGCCAATTCCCGCGGAGGAGACTCCGAGAGATGAGCCGGC

Acidothermus cellulolíticus 11B SAM-I aptamer domain (Ac):
Genbank genome accession CP000481.1, nucleotides 103255..103416
ccaagtaatacgactcactata**GG**CCGCTCATCGAGAGGGGCTGAGGGACCGGCCCGGTGAAGCCCCGGCAACCGTCAC
GGCGGTGTGGACGCCGAAGAGGCGCTGGAGTTGCGGCGCCAACGCGAGGCCACGTCGTGATCGGTGCCAAATCC
GGCCTGCGGAAGGTCCGCGGGGAAGATGAGGAG

Carboxydothermus hydrogenoformans Z-2901 SAM-I aptamer domain (Ch):
Genbank genome accession CP000141.1, nucleotides 2169981..2169871
ccaagtaatacgactcactata**GG**CGCCTCTTATCAAGAGTGGCGGAGGGACTGGCCCAATGAAGCCCGGCAACCGGCC
ATATTTTTGGCAATGGTGCCAATTCCTGCGGATTAAATTCCGGGAGATAAGAGGAG

Polaribacter sp. MED152 SAM-I aptamer domain (Ps):
NCBI reference sequence NZ_CH902588.1, nucleotides 1408674..1408551
ccaagtaatacgactcactata**GG**GAAATGTTATCAAGAAAGGTGGAGGGATTAGACCCATTGAAGCCTTAGCAACCCTT
TAGAAATAAAGAAGGTGCTAAATTCTACTCTTTTAAATTGTTTAATTTAAAAGGATAGATAACAAAAG

Table S1: Primer Sequences

EXPERIMENT		NOTES
NAME		
	Bs SAM-I WT	
SH19	ccaagtaatacgactcactata**GG**GTTCTTATCAAGAGAAGCAGAGGG	For
SH20	CTCTTCTTATCTTCCAAGCTGTTCGAG	Rev
	Bs SAM-I M1	
SH21	ccaagtaatacgactcactata**GG**GTTCTTATCAAGAGAAGCAGAGGGA CTCCCCCGACGAAGCTTCAGCAACCGGTGTAATGGCGATCAGCCA TGACCAAGGTGCTAAATCCAGCAAGCTCGAACAGCTTGGA AGATAAGAAGAG	For (Primer extension)
SH19	See above	For (Template amplification)
SH20	See above	Rev
	Bs SAM-I P2	
SH22	ccaagtaatacgactcactata**GG**GTTCTTATCAGAAGAAGCAGAGGGA CTGGCCCGACGAAGCTTCAGCAACCGGTGTAATGGCGATCAGCC ATGACCAAGGTGCTAAATCCAGCAAGCTCGAACAGCTTGGAAGAT	For (Primer extension)

	AAGAAGAG	
SH23	ccaagtaatacgactcactata**GG**GTTCTTATCAGAAGAAGCAGAGGG	For (Template amplification)
SH20	See above	Rev
	Bs SAM-I M1N	
QQ45	TGACACGAAAATTTCATATCCGTTCTTATCAGAAGAAGCAGAGGGACTG	For (Quikchange)
QQ46	CAGTCCCTCTGCTTCTTCTGATAAGAACGGATATGAAATTTTCGTGTCA	Rev (Quikchange)
	Bs SAM-I P2N	
QQ43	CAAGAGAAGCAGAGGGACTCCCCCGACGAAG	For (Quikchange)
QQ44	CTTCGTCGGGGGAGTCCCTCTGCTTCTCTTG	Rev (Quikchange)
	Pi SAM-I	
SCW13	ccaagtaatacgactcactata**GG**GAAATGTTATCAAGAAAGGCGGA	For
SCW14	TTTTTGTTATCTATCCAATTACGAATAATTG	Rev
	Rx SAM-I	
SCW7	ccaagtaatacgactcactata**GG**GGGCGCTCATCGAGAG	For
SCW8	GCCGGCTCATCTCTCG	Rev
	Ac SAM-I	
SCW3	ccaagtaatacgactcactata**GG**CCGCTCATCGAGAGGG	For
SCW4	CTCCTCATCTTCCCCGC	Rev
	Ch SAM-I	
SCW1	ccaagtaatacgactcactata**GG**CGCCTCTTATCAAGAGTGG	For
SCW2	CTCCTCTTATCTCCCGGAA	Rev
	Ps SAM-I	
SCW11	ccaagtaatacgactcactata**GG**GAAATGTTATCAAGAAAGGTGGAG	For
SCW12	CTTTTGTTATCTATCCTTTTAAATTAAACAA	Rev

Selection Criteria and Computational Analysis of Putative SAM-I Riboswitches

A Perl program was developed to integrate, calculate, and analyze sequence specific statistics for a library of 1,182 putative SAM-I riboswitches from at least 93 different host organisms. Alignment and familial data was provided by the Rfam database (accession RF00162, http://rfam.sanger.ac.uk/) and used as inputs.[15] The two datasets were cross-referenced and parsed from the raw data files. Statistics specific to each sequence regarding its accession number, organism, bit score, energetic stability based on its secondary structure, length, direction within the genome, overall GC content, and GC content per length of secondary structural elements (e.g. P1 stem) were generated for each sequence and tabulated in an Excel spreadsheet. RNAeval of the VIENNA software package was used to calculate energies.[16]

Approximately 36% of the sequences in the alignment dataset were omitted because they could not be automatically linked to a corresponding entry within the familial SAM dataset and thus were missing the bit score, which provides a measure of how well the sequence matches the covariance model compared to the null model.[17] Typical bit scores of remaining sequences range from 32.3 to 106.5, with a high bit score indicating a better match to the covariance model. An additional 4% of the sequences were disregarded due to overly large predicted energy values (~9999 kcal/mole). This was generally caused by putative P3 or P4 hairpin loops less than 3 nucleotides in length, which is likely due to misalignment or misidentification. Typical energy values of remaining sequences range from -36.25 to 9.76 kcal/mol. Low energy values indicate a higher thermodynamic stability for the putative secondary structure and usually correlated with high GC content.

The remaining 730 sequences were evaluated based upon the following criteria: bit score, energy, GC content, organism, and sequence alignment of discrete secondary structural elements. Fifteen candidates were manually selected for variation rather than conformity in their statistics (e.g. low and high bit scores; growth at cold, moderate, and high temperatures; low, moderate, and high GC content) and checked for reasonable alignment to the consensus secondary structure. After manual verification of the downstream gene as related to SAM metabolism, five of these candidates were selected for biochemical analysis along with the previously validated *yitJ* SAM-I riboswitch from *Bacillus subtilis*.

Sequence #	Accession #	Family	Bit Score	Thermophilic?	Energy (kcal/mol)	Sequence Length	Direction	GC(%)
1	CP000481.1	Acidothermus cellulolyticus	46	Y	-24.87	156	F	70
14	CP000386.1	Rubrobacter xylanophilus	59.78	Y	-34.43	112	R	74
25	AANA01000001.1	Polaribacter sp.	58.66	N	-13.81	118	R	31
26	AAOG01000001.1	Polaribacter irgensii	71.63	N	-16	110	R	35
133	Y09476.1	Bacillus subtilis	97.43	N	-21.01	118	R	50
1050	CP000141.1	Carboxydothermus hydrogenoformans	104.3	Y	-30.2	105	R	52

Sequence #	P1 Length	P1 GC(%)	P2 Length	P2 GC(%)	P2a Length	P2a GC(%)	P3 Length	P3 GC(%)	P4 Length	P4 GC(%)
1	12	50	6	100	6	100	18	72	8	88
14	16	62	6	83	6	100	18	89	8	75
25	16	25	6	83	6	100	18	56	8	50
26	16	25	6	100	6	100	18	56	8	50
133	16	25	6	67	6	100	18	67	8	50
1050	16	38	6	100	6	100	18	83	8	75

Sequence #	Sequence	Putative Secondary Structure
1	..CUCAUCGAGAGGGGCUGAGGGACCGGCCCGGUGAAGCCCCGGCAACCGUCACGGCGGUGUGGACGCCGAAGAGGCGCU GGAGUUGCGGCGCCAACGCGAGGCCACGUCGUGAUCGGUGCCAAAUCCGGCCUGCGGAAGGUCCGCGGGGAAGAUGAG..	(((((((((.....(((...(((.....)))).....)))..(((.((((((.....))).)))))).....((((.....))))...)))))))))
14	CGCUCAUCGAGAGCGGUGGAGGGACGGGCCCUGCGAAGCCGCGGCAACCGGCGGGCGGCGGACGCCCGCGCCAGGUGCC AAUUCCCGCGGAGGAGACUCCGAGAGAUGAGCC	(((((((((.....(((...(((.....)))).....)))..(((.((((((.....))).)))))).....((((.....))))...)))))))))
25	AUGUUAUCAAGAAAGGUGGAGGGAUUAGACCCAUUGAAGCCUUAGCAACCCUUUAGAAAUAAAGAAGGUGCUAAAUU CUACUCUUUUAAAUUGUUUAAUUUAAAAGGAUAGAUAACAA	(((((((((.....(((...(((.....)))).....)))..(((.((((((.....))).)))))).....((((.....))))...)))))))))
26	AUGUUAUCAAGAAAGGCGGAGGGAUUAGACCCAUUGAAGCCUUAGCAACCCUUUAGUAAUAAAGAAGGUGCUAAAUU CUACUCAAUUAUUCGUAAUUGGAUAGAUAACAA	(((((((((.....(((...(((.....)))).....)))..(((.((((((.....))).)))))).....((((.....))))...)))))))))
133	UUCUUAUCAAGAGAAGCAGAGGGACUGGCCCGACGAAGCUUCAGCAACCGGUGUAAUGGCGAUCAGCCAUGACCAAGG UGCUAAAUCCAGCAAGCUCGAACAGCUUGGAAGAUAAGAA	(((((((((.....(((...(((.....)))).....)))..(((.((((((.....))).)))))).....((((.....))))...)))))))))
1050	CUCUUAUCAAGAGUGGCGGAGGGACUGGCCCAAUGAAGCCCGGCAACCGGCCAUAUUUUUGGCAAUGGUGCCAAUUCC UGCGGAUUAAAUUCCGGGAGAUAAGAG	(((((((((.....(((...(((.....)))).....)))..(((.((((((.....))).)))))).....((((.....))))...)))))))))

Sequence #	Checked Alignment Quality	Downstream Gene
1	Yes	L-threonine synthase (AceI_0100)
14	Yes	Homocysteine S-methyltransferase (RxyI_0843)
25	Yes	Not found
26	Yes	O-acetylhomoserine sulfhydrylase (PI23P_02107)
133	Yes	Methylene tetrahydrofolate reductase (*YitJ*)
1050	Yes	Putative ABC transporter (CHY_2422)

Tables 1-3 (top to bottom): Sample program output for selected sequences; Table 4 (bottom): User criteria evaluation of selected sequences

SI Bibliography

(1) Wickiser, J. K.; Cheah, M. T.; Breaker, R. R.; Crothers, D. M. *Biochemistry* **2005**, *44*, 13404.

(2) Wickiser, J. K.; Winkler, W. C.; Breaker, R. R.; Crothers, D. M. *Mol. Cell* **2005**, *18*, 49.

(3) Giddings, J. C. *Unified Separation Science*; Wiley New York: New York, 1991.

(4) Regulski, E. E.; Breaker, R. R. *Methods Mol. Biol.* **2008**, *419*, 53.

(5) Rio, D. C.; Ares, M.; Nilsen, T. W. *RNA: A laboratory manual*; Cold Spring Harbor Laboratory Press, 2010.

(6) Willkomm, D.; Hartmann, R.; Bindereif, A.; Schon, A.; Westhof, E. *Handbook of RNA Biochemistry*; Wiley, 2005; Vol. 1.

(7) ThermoFisherScientific In *http://www.piercenet.com/files/TR0031-Calc-FP-ratios.pdf;* Pierce Biotechnology: Rockford, 2011.

(8) Wood, B. In *http://tools.invitrogen.com/content/sfs/COAPDFs/2012/1141015_A30634.pdf;* Probes, M., Ed.; Life Technologies Corporation: 2011.

(9) Invitrogen In *http://www.invitrogen.com/etc/medialib/en/filelibrary/cell_tissue_analysis/pdfs.Par.87420.File.tmp/O-063190-Alexa-Fluor-SelectionGuide.pdf;* Molecular Probes: invitrogen detection technologies: 2005.

(10) Goodrich, J. A.; Kugel, J. F. *Binding and Kinetics for Molecular Biologists*; Cold Spring Harbor Laboratory Press: New York, 2007.

(11) Hou, C.; Herr, A. E. *Anal. Chem.* **2010**, *82*, 3343.

(12) Rathore, A. S.; Horváth, C. *Electrophoresis* **1997**, *18*, 2935.

(13) Winkler, W. C.; Nahvi, A.; Sudarsan, N.; Barrick, J. E.; Breaker, R. R. *Nat. Struct. Biol.* **2003**, *10*, 701.

(14) Heppell, B.; Lafontaine, D. A. *Biochemistry* **2008**, *47*, 1490.

(15) Griffiths-Jones, S.; Bateman, A.; Marshall, M.; Khanna, A.; Eddy, S. R. *Nucleic acids research* **2003**, *31*, 439.

(16) Hofacker, I. L.; Fontana, W.; Stadler, P. F.; Bonhoeffer, L. S.; Tacker, M.; Schuster, P. *Monatshefte für Chemie/Chemical Monthly* **1994**, *125*, 167.

(17) Nawrocki, E. P.; Kolbe, D. L.; Eddy, S. R. *Bioinformatics* **2009**, *25*, 1335.